Multispectral Detection of Fecal Contamination on Apples Based on Hyperspectral Imagery: Part I. Application of Visible and Near–Infrared Reflectance Imaging

M. S. Kim, A. M. Lefcourt, K. Chao, Y. R. Chen, I. Kim, D. E. Chan

Abstract. *Fecal contamination of apples is an important food safety issue. To develop automated methods to detect such contamination, a recently developed hyperspectral imaging system with a range of 450 to 851 nm was used to examine reflectance images of experimentally contaminated apples. Fresh feces from dairy cows were applied simultaneously as a thick patch and as a thin, transparent (not readily visible to the human eye), smear to four cultivars of apples (Red Delicious, Gala, Fuji, and Golden Delicious). To address differences in coloration due to environmental growth conditions, apples were selected to represent the range of green to red colorations. Hyperspectral images of the apples and fecal contamination sites were evaluated using principal component analysis with the goal of identifying two to four wavelengths that could potentially be used in an on–line multispectral imaging system. Results indicate that contamination could be identified using either three wavelengths in the green, red, and NIR regions, or using two wavelengths at the extremes of the NIR region under investigation. The three wavelengths in the visible and near–infrared regions offer the advantage that the acquired images could also be used commercially for color sorting. However, detection using the two NIR wavelengths was found to be less sensitive to variations in apple coloration. For both sets of wavelengths, thick contamination could easily be detected using a simple threshold unique to each cultivar. In contrast, results suggest that more computationally complex analyses, such as combining threshold detection with morphological filtering, would be necessary to detect thin contamination spots using reflectance imaging techniques.*

Keywords. *Hyperspectral imaging, Multispectral imaging, Reflectance, Fecal contamination.*

Unpasteurized apple juice or cider, a major beverage for children in the U.S., has been identified as a repeated source of *E. coli* O157:H7 infection. The U.S. Food and Drug Administration has recently issued a report summarizing health risks and remediation measures associated with the safe and sanitary processing of fruit juices, which identifies a critical need to develop methods for detection of fecal contamination of apples (FDA, 2001). Animal feces, particularly bovine feces, are the most likely source of pathogenic *E. coli* contamination of apples. The contamination potential is increased with physical damage such as lesions and bruises, which provide an ecological niche for bacterial growth (Burnett et al., 2000; Mercier and Wilson, 1994). Reported sources of fecal contamination of apples include cows, deer, and humans (Cody et al., 1999).

Article was submitted for review in January 2002; approved for publication by the Information & Electrical Technologies Division of ASAE in August 2002.

Company and product names are used for clarity and do not imply any endorsement by the USDA to the exclusion of other comparable products.

The authors are **Moon S. Kim,** Research Physicist, **Alan M. Lefcourt, ASAE Member Engineer,** Research Biomedical Engineer, **Kevin Chao, ASAE Member Engineer,** Research Agricultural Engineer, **Yud–Ren Chen, ASAE Member Engineer,** Research Leader, and **Diane E. Chan,** Agricultural Engineer, USDA–ARS Instrumentation and Sensing Laboratory, Henry A. Wallace Beltsville Agricultural Research Center, Beltsville, Maryland; and **Intaek Kim,** Associate Professor, Department of Information Engineering, Myongji University, Yongin, Kyonggido, South Korea. **Corresponding author:** Moon S. Kim, USDA–ARS–ISL, Bldg 303 BARC–East, 10300 Baltimore Ave., Beltsville, MD 20705–2350; phone: 301–504–8450; fax: 301–504–9466; e–mail: kimm@ba.ars.usda.gov.

Spectral sensing techniques are commonly used for inspection of anomalies in food commodities. These non–invasive techniques include machine vision and multispectral imaging; the most commonly used spectral regions range through the visible (VIS) to the near–infrared (NIR). A number of investigators have demonstrated the applications of these techniques to the detection of defects on apples as well as physical properties such as size and color (Miller et al., 1998; Upchurch et al., 1990; Upchurch et al., 1994; Tao, 1997; Throop et al., 1995). Until recently, implementations of spectral and imaging technologies have generally concentrated on the quality assessment of fruits. However, interest in addressing food safety issues is increasing.

Hyperspectral imaging methods, which combine the features of imaging and VIS/NIR spectroscopy to simultaneously acquire spatial and spectral information, have gained the interest of researchers as a powerful tool in identifying and detecting spectral and spatial anomalies due to defects and contamination on agricultural products. Recently, researchers at the USDA–ARS Instrumentation and Sensing Laboratory (ISL) in Beltsville, Maryland, developed a laboratory–based hyperspectral imaging system capable of both reflectance and fluorescence sensing (Kim et al., 2001a). Because a complete spectral profile is associated with each image pixel, the resulting data quantity makes on–line use of hyperspectral images impractical. Instead, the hyperspectral data can be used to determine optimal wavelengths for multispectral imaging systems. The multispectral imaging approach is favorable when considering the stringent constraints imposed by speed requirements for real–time processing (Lu and Chen, 1998; Kim et al., 2001a;

Mehl et al., 2002). Several types of common aperture systems that allow multispectral (two to four spectral bands) imaging of samples with a single acquisition are readily available (Chen et al., 2002).

There are two main objectives of this study: to present a systematic method for using hyperspectral data to identify wavebands to be used in multispectral detection systems, and to evaluate spatial and spectral responses of hyperspectral reflectance images of fecal–contaminated apples. In agricultural production systems, the time available to evaluate individual units normally ranges from tenths to hundredths of a second. Numerous commercial systems based on multispectral imaging for reflectance measurements meet these time requirements. However, selection of the wavebands used for such systems is often based on relatively unsophisticated considerations, such as availability of RGB cameras or knowledge of minimum or maximal reflectance bands. A method for systematic identification of the optimal number and location of wavebands based on hyperspectral image data does not exist. In this study, principal component analysis (PCA) is used to aid in visualizing the hyperspectral data and to develop criteria for selection of wavebands for multispectral detection. This methodology will be applied to hyperspectral images of fecal–contaminated apples with the goal of identifying two to four wavebands that could be used in an on–line system.

Materials and Methods

Hyperspectral Imaging System

The ISL hyperspectral imaging system is composed of four critical components: a sample transport system, lighting, optics, and a camera. A conveyor belt is used to transport sample materials through a line of sensor field–of–view in a transverse direction. Line–by–line scans of spatial–by–spectral data are combined sequentially to construct a volume of spatial–spectral data. The laboratory–based system was operated in a darkened room to minimize interference from scattered or ambient radiation. Sample illumination for reflectance measurements was provided by two 150 W halogen lamps powered by regulated DC power supplies. Light is transmitted through two fiber optic bundles to randomly arranged rectilinear fiber bundles (Fiber–Lite A–240P, Dolan–Jenner Industries, Lawrence, Mass.), which provide near–uniform sample illumination.

A uniform radiometric response throughout the spatial and spectral domains was obtained by calculating reflectance factors (RF), which are the ratios of reflected radiation from a sample to those of a known reference material under the same illumination. A white Spectralon panel (approximately 99% reflectance) was used as the reference. RF values ranged from 0.0 to 1.0. To preserve the resolution of image data, RF values were multiplied by 10000 prior to storage.

The effective resolution of the camera and optics was 408 × 256 pixels by 16 bits. To increase throughput and the signal–to–noise ratio, images were binned by two in the spectral dimension, which resulted in 128 spectral channels (approximately 3.6 nm channel interval) per spatial pixel. Due to inefficiencies of the system at certain wavelength regions (e.g., light output in the blue <450 nm and CCD quantum efficiency in the NIR >850 nm), only the wavelength range from 450 to 851 nm (110 channels) was used in this investigation. For a detailed description of the ISL hyperspectral imaging system, refer to Kim et al. (2001a).

Sample Materials

Four cultivars of apples (Red Delicious, Gala, Fuji, and Golden Delicious) were used. To address differences in coloration due environmental growth conditions, apples were selected to represent the range of green to red colorations. To mimic different possible thickness of fecal contamination, feces were applied to apples as a thick patch or as a thin, semi–transparent smear (not readily visible to the human eye).

Apples were selected from crates of apples that were harvested the previous season (1999) in Pennsylvania (Rice Fruit Co., Gardners, Pa.), and kept in a cold storage room (2° C to 4° C). Within each cultivar, individual apples display color variations due mainly to environmental growth conditions such as solar exposure. For instance, sun–exposed apples ripen faster than apples with less exposure to direct solar radiation. Apple sides showing near–uniform color were classified as sun–exposed, while apple sides showing red–green variegations or green color were classified as shaded. Four apples were selected for each of the four cultivars such that the apples represented the full range of normal color variation. A total of 16 apples was used in this study.

Fresh feces were obtained from a pasture at the USDA Beltsville dairy. Two spots of feces were applied to one side of each apple. One spot was a 2 mm thick patch, while the second was a thin, transparent smear. A spatula was used to evenly apply fecal matter on the apple surface to create the thick patch, while a ball of fecal matter was lightly pressed against an apple surface and removed to create the thin smear. Both spots were approximately 1 cm in diameter. For scanning, four treated apples per cultivar were placed on a tray painted with non–fluorescent, flat black paint to minimize background scattering. Two from each image are shown in the figures for brevity.

Data Processing and Analysis

Software was developed using Visual Basic (Microsoft, Seattle, Wash.) to correct and convert the individual raw data files downloaded from the camera into 16–bit hyperspectral images. The software includes functions to allow image visualization/enhancement, simple threshold classification, gray–scale image stretch, band arithmetic operations, and spectral and spatial data retrieval. Processed images or spectra were saved as a standard 8–bit bitmap and ASCII files for presentation purposes, and in the data file format required by the commercial software ENVI (Environment for Visualizing Images, Version 3.2, Research Systems Inc., Boulder, Colo.). ENVI software was used for further analyses including PCA.

Individual images at several wavelengths were contrasted with spectra of the contaminated and sample surfaces to study the effects of spatial variations within a wavelength and across spectral responses. The PCA was used to reduce spectral dimensionality of the hyperspectral reflectance images, and to determine the several dominant spectral regions responsible for discriminating uncontaminated apple surfaces from spots contaminated with feces. A simple threshold applied to one of the NIR band images (e.g., 851

nm) was used to create a mask for the four apple surfaces in each image. The threshold value was determined visually for each cultivar to exclude the background. Only the sample surfaces were subjected to PCA to discriminate the uncontaminated surface areas from contaminated areas.

Subsequently, individual principal component (PC) images were visually evaluated to determine PC images with (1) the least variation in uncontaminated sample surfaces and (2) the largest contrast between contaminated spots and sample surfaces. These PC images were also subjected to a simple threshold classification to discriminate the uncontaminated surface areas from the contaminated areas. Each PC image is a linear sum of the original images at individual wavelengths multiplied by corresponding (spectral) weighing coefficients. Two to three wavelengths with high (local maxima) weighing coefficients from the PC image best meeting the above criteria were selected as the dominant wavelengths. Principal components (images) using only the selected dominant wavelengths (multispectral images) were re–calculated.

Results and Discussion

Hyperspectral Reflectance Images

Figure 1 shows representative images of Red Delicious apples at 450 (R450), 550 (R550), 649 (R649), and 851 nm (R851), respectively. For each wavelength, the lower apple image is a shaded side (i.e., variegated, red and green colorations), and the upper image is a sun–exposed side (near uni-form red coloration). The two plots adjacent to each set of images illustrate spatial variations in intensity values (percent reflectance) along the dotted vertical lines in the image. The left plot corresponds to the left dotted line in the image, and the right plot corresponds to the dotted line on the right. The left and right dotted lines also transect the thick and thin feces–treated spots on the apples, respectively, to illustrate the changes in intensities due to fecal contamination. The intensities (brightness) of the shaded Red Delicious apples in the VIS region are higher compared to those of the sun–exposed apples (fig. 1). The R550 image exhibited the most substantial intensity differences between the shaded and sun–exposed sides. In addition, the variegated features of the shaded side were more pronounced at R550 compared to the other spectral band images. These differences result from variations in plant constituents, such as chlorophyll and carotenoid species, that exhibit strong absorption characteristics in this region of the spectrum. In contrast, apples lack light absorbing constituents in the NIR region <850 nm, and hence, a greater portion of the incident light is scattered. This lack is evident in the R851 image, where both the sun–exposed and shaded images show similar reflectance intensities and have higher reflectance compared to the corresponding VIS images.

Specular reflectance characteristics were observed near the center portions of the apples. These are further evident as abrupt spikes in the spatial profile plots. Furthermore, decreases in reflectance from near the center portions of

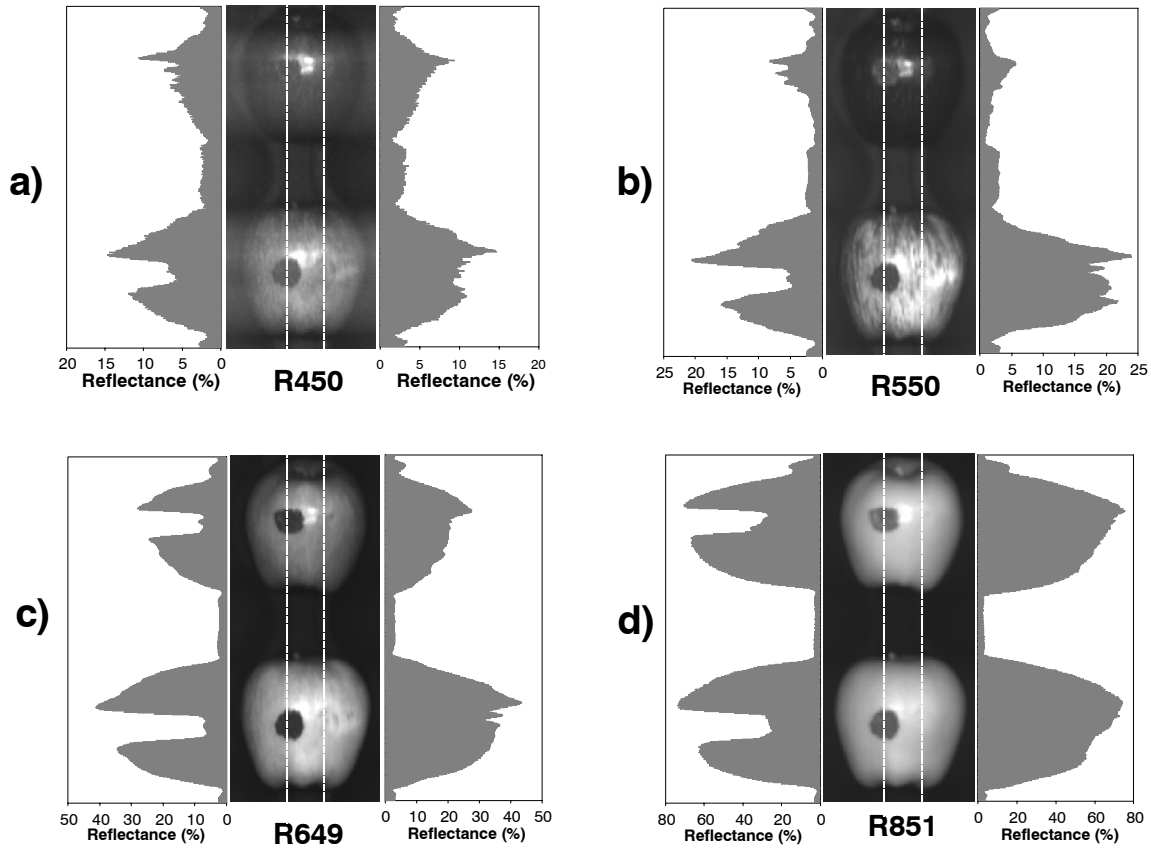

Figure 1. Reflectance images of feces–treated Red Delicious apples at (a) 450 nm, (b) 550 nm, (c) 649 nm, and (d) 851 nm. Each image is accompanied by spatial profile plots for the dotted vertical lines. Note that images were acquired with four apples, but only two apples, shaded (lower image) and sun–exposed (upper image), are shown.

apples to the edges were seen. These observations suggest that the surface morphology (target depth and directional factors), along with illumination and sensor view angles, affected the reflectance measurements of the apples. Regardless of spatial variations in intensities across the apple surfaces, the thick feces treatment was clearly evident as a dark round spot in all four images of the shaded apple and in the R649 and R851 images of the sun–exposed apple. However, the thick feces spot on the sun–exposed apple was not clearly evident in the R450 image and appeared lighter at R550. For the thin smears, the reflectance spatial profiles at R450 for the sun–exposed apple showed slightly higher intensities compared to the uncontaminated apple surfaces, but this reflectance was lower than that of the uncontaminated surfaces of the shaded apple. These observations indicate that a thin feces cover on apples may not be easily detected with the use of individual bands. For cultivars other than Red Delicious, the color differences between sun–exposed and shaded side apples were not as prominent, and hence, images for the other cultivars are not shown for brevity. Similar effects of heterogeneity of reflectance intensities over the apple surfaces and feces spots were observed.

VIS/NIR Reflectance Spectra

Representative reflectance spectra of Fuji, Gala, Golden Delicious, and Red Delicious including sun–exposed and shaded sides, and thin and thick feces–treated spots for each cultivar are presented in figures 2a, 2b, 2c, and 2d, respectively. These spectra were extracted from the hyperspectral image data and are an average of four spectra (one per apple), each obtained from a rectangular region of interest (ROI) containing approximately 10 × 10 pixels per treatment, except for sun–exposed and shaded apple surface spectra in which two ROIs per apple were used to obtain the mean spectra. The two ROIs for the uncontaminated apples spectra were located near the center portion, adjacent to the feces spots of the samples.

Spectra in the VIS region (i.e., 500 nm to 700 nm) depicted the cultivar and growth environment–dependent variations in apple colorations (pigments). The shaded apple spectra showed higher reflectance in the green region of the spectrum compared to the sun–exposed apple surfaces. One common feature observed in the apple spectra is absorption of chlorophyll *a* at approximately 675 nm. In general, the thin feces treatment appeared to maintain spectral shapes of normal apple surfaces, but slightly lowered the relative reflectance intensities. The thick fecal treatment on four cultivars showed nearly identical spectral characteristics, indicating that most of the incident light did not penetrate the feces patches to the apple surfaces. These feces spectra also exhibited an absorption characteristic of chlorophyll *a* at 675 nm. Kim et al. (2001b) suggested that plant constituents in cow feces including chlorophyll *a* and metabolites such as

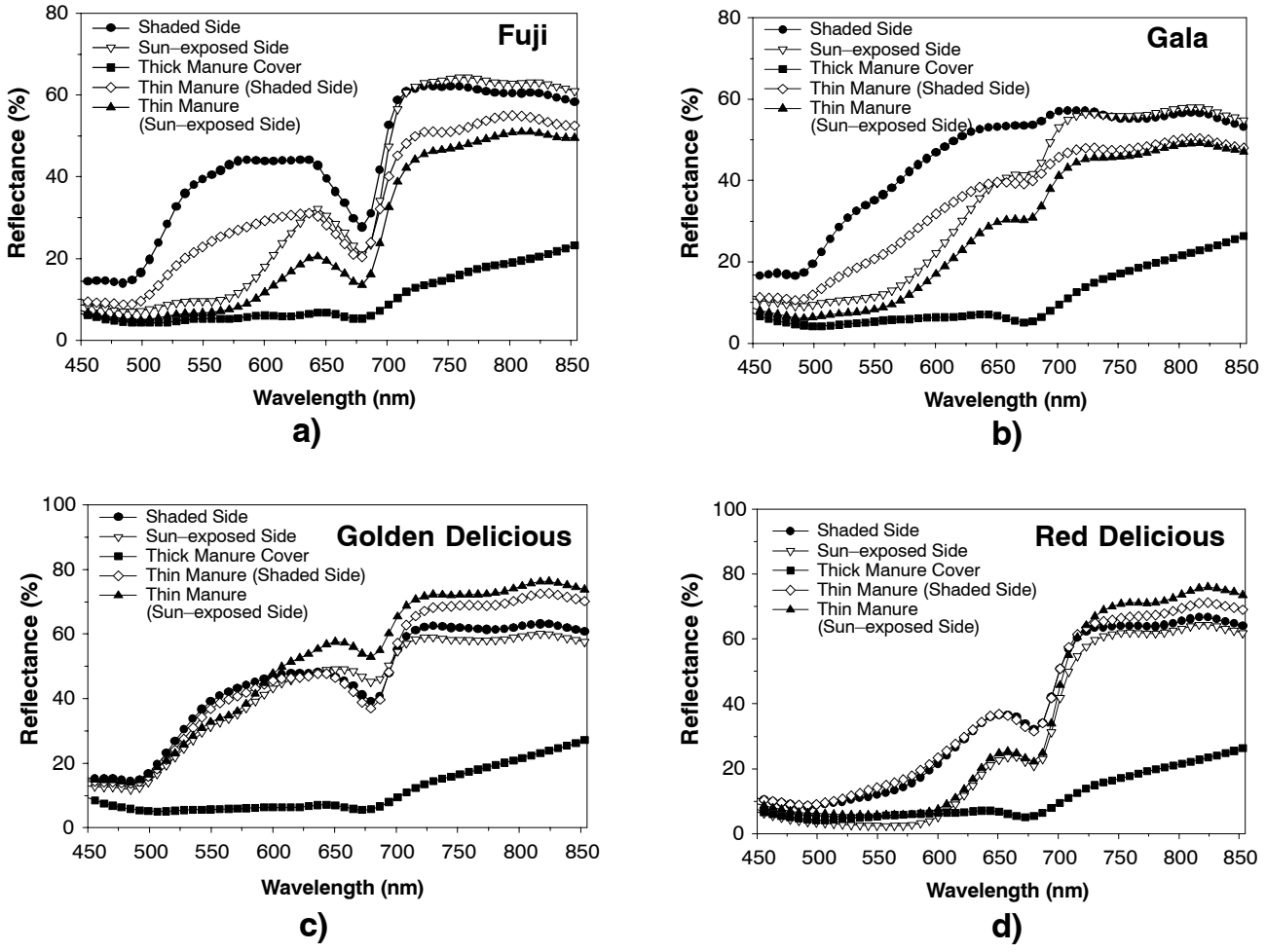

Figure 2. Reflectance spectra of the feces–treated and sample surfaces extracted from the hyperspectral image data for (a) Fuji, (b) Gala, (c) Golden Delicious, and (d) Red Delicious apples.

pheophobite *a* may be responsible for these observations. Apple surfaces exhibited flat reflectance responses (a plateau), while the thick feces treatment showed a monotonic increase in intensities in the NIR region from approximately 730 to 850 nm. A slight slope change in this region of the spectrum was also observed in the spectra of the thin fecal treatment on shaded and sun–exposed sides of Fuji (fig. 2a).

An exogenous contaminant such as fecal matter alters spectral characteristics of the apple by blocking or attenuating the light reaching the apple surfaces. The spectral properties of the contaminant also affect reflectance measurements, particularly when the spectral properties are significantly different from those of the underlying substrate, as is the case for feces on apple surfaces (fig. 2). These differences provide a basis for detection of contaminated areas. However, when the fecal contaminant was thinly applied, so that the apple skin was visible through the thin smear, spectral changes were less apparent compared to those of thick feces. In addition, the spectra shown in figure 2 do not account for the spatial variations (decreases) in intensities from the center portions toward the edges. Because of these problems, a single (monochromatic) band in the VIS/NIR may not be adequate for detection of contaminated spots, especially the thin feces spots on the apple surfaces.

PCA of Hyperspectral Images in the VIS to NIR Regions

The first six PC images obtained by using all 110 spectral channels (450 to 851 nm) are shown in figures 3a, 3b, 3c, and 3d for Fuji, Gala, Golden Delicious, and Red Delicious, respectively. Features such as color variegations, lenticels, and thin fecal covers not readily visible in the individual images are more apparent in these images. Note that while acquiring images for Fuji, the placement of apples for shaded and sun–exposed sides were reversed, and hence, the top and bottom represent sun–exposed and shaded side, respectively. In the first principal component (PC–1) images, intensity decreases from the center to the edges of apples, and the thick feces spots are evident. The PC–2 images appear to accentuate differences in colorations between shaded and sun–exposed sides. In the PC–3 images, the effects of fecal treatment are observed with less spatial variation in intensities for uncontaminated apple surfaces. The fourth component images mainly illustrate the specular effects in the center portions of the apples. The nature of the PCA is that the largest variance of the hyperspectral reflectance images is accounted for in the PC–1 images, followed by the subsequent PC images. Hence, only small effects or details are normally apparent in higher–order images. In this study, information from PC images higher than third order did not improve discrimination of contamination spots.

Based on visual assessment, the PC–3 images for all cultivars appeared to provide the best discrimination between the feces–treated spots and uncontaminated apple surfaces regardless of apple coloration. In order to further test this observation, a simple threshold method was applied to the PC images (first to sixth PC images) in an attempt to classify contamination spots. Figure 4 illustrates key steps involved in performing the simple threshold classification for the feces–treated spots using the PC–3 image of a Red Delicious apple. First, a mask image for the apple (fig. 4a) was created using an NIR band (851 nm) image. Then average histograms (fig. 4c) of masked images (fig. 4b) for each PC from 1 to 6, by cultivar, were examined to determine simple thresholds that allowed discrimination of contaminated spots from the uncontaminated apple surfaces. The threshold value to classify the feces spots for individual cultivars was determined so that none of the pixels for uncontaminated apple surfaces were classified in the resultant binary classification image (fig. 4d), except for stems. The spectral characteristic of the stems resembled that of the thick fecal samples, and because of this, stems were allowed to be classified along with the treated spots. Using this approach, it was confirmed that the PC–3 images allowed the best discrimination between the feces spots and apple surfaces.

PCA of Hyperspectral Images in the NIR Region

The color variations of uncontaminated apple surface mainly affected the VIS region of the spectrum. Thus, avoidance of VIS region data may eliminate the effects of reflectance variations of apples due to variation in colorations within and between apples. The region where the transition from red to NIR (also know as "red edge") occurs is approximately from 700 to 750 nm. Therefore, wavelengths from 748 to 851 nm (29 spectral channels) were used to construct PC–1 to PC–6 for NIR hyperspectral images.

Figure 5 shows the resultant PC–1 and PC–2 images. The PC–1 images yielded effects similar to those observed in the VIS–NIR PC–1 (fig. 3), i.e., the decreases in intensity from the center portions to the edges of apples were mainly expressed in the PC–1 images. The PC–2 images displayed the best contrast between the treated spots and the apples surfaces for all the cultivars. The third column of figure 5 for individual cultivars illustrates the resultant simple threshold classification for the PC–2 images. Using PC–2 images, 16 of 16 thick spots and 16 of 16 thin spots were discriminated from normal apple surfaces. However, the classified pixels under the thin smears were significantly fewer than the number of pixels covering the actual smear spots and were also fewer compared to the thick spots. Some stems were also classified as contamination (false positive).

Selection of Optimal Spectral Bands

Figure 6a shows weighing coefficients for the PC–3 obtained by using images across the entire spectral region. The PC–3 weighing coefficients for all cultivars indicated wavelengths in the green, red, and NIR as the dominant factors responsible for generating the PC–3. The weighing coefficients for the PC–2 obtained using only the NIR region (fig. 6b) show two common wavelengths for all cultivars, at the beginning and the end of the NIR spectral region. It is evident that the PC–2 depicted the NIR slope differences between the feces and apples observed in figure 2, and the PC–2 weighing coefficients confirmed that the shortest and longest bands in the NIR region resulted in the largest slope differences between the contamination spots and the apple surfaces.

Based on the above results, several optimal spectral bands for use in a multispectral detection scheme were selected. Table 1 summarizes the wavelengths for individual cultivars obtained from the weighing coefficients of the PC–3 from the full spectrum and of the PC–2 from the NIR region. Note that two common wavelengths (748 and 851 nm) were singled out, regardless of cultivar, based on the weighing coefficients for the PC–2.

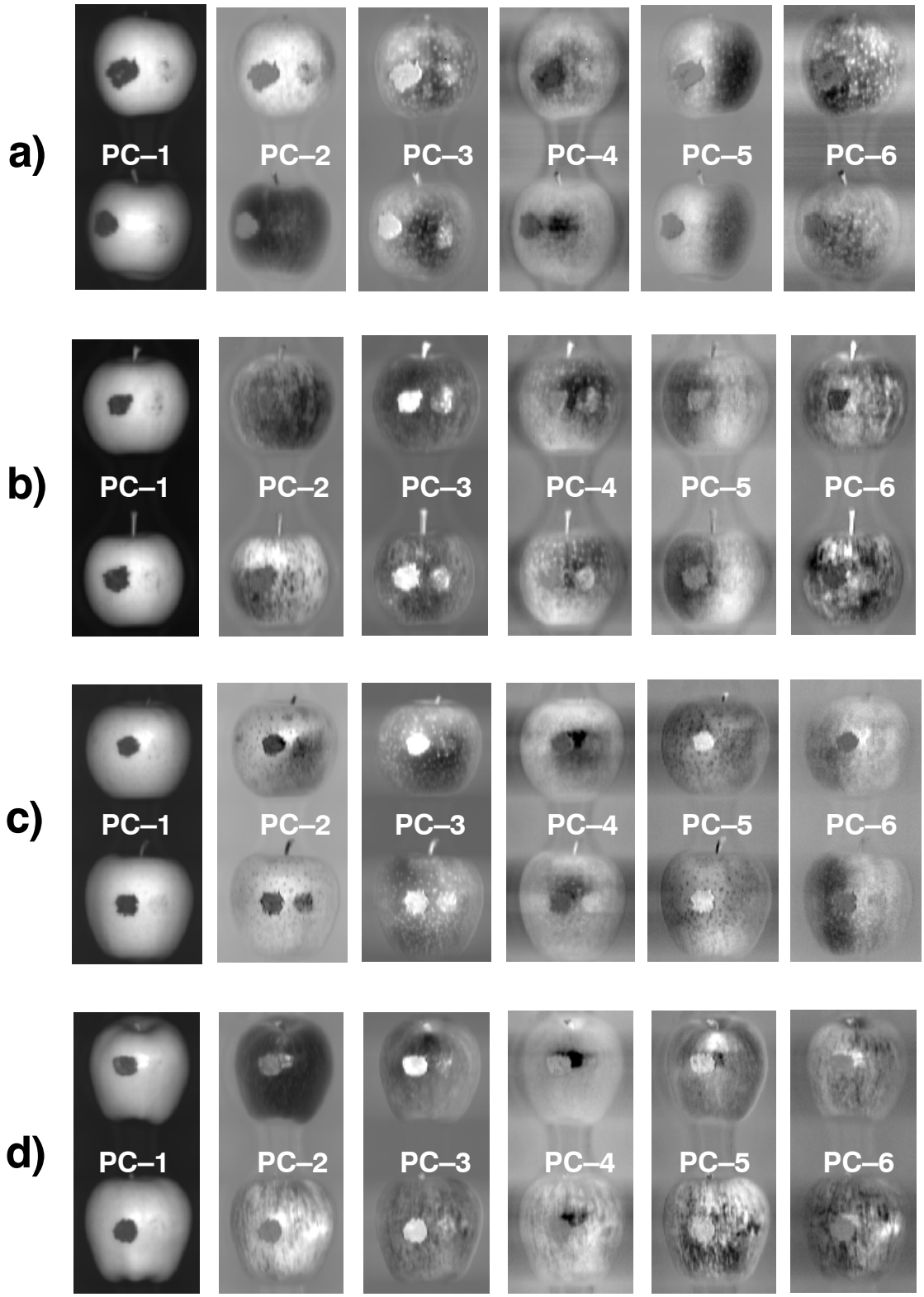

Figure 3. First to sixth principal component images obtained using the entire spectral regions from 450 to 851 nm (110 spectral channels) of the hyperspectral reflectance image data for (a) Fuji, (b) Gala, (c) Golden Delicious, and (d) Red Delicious apples.

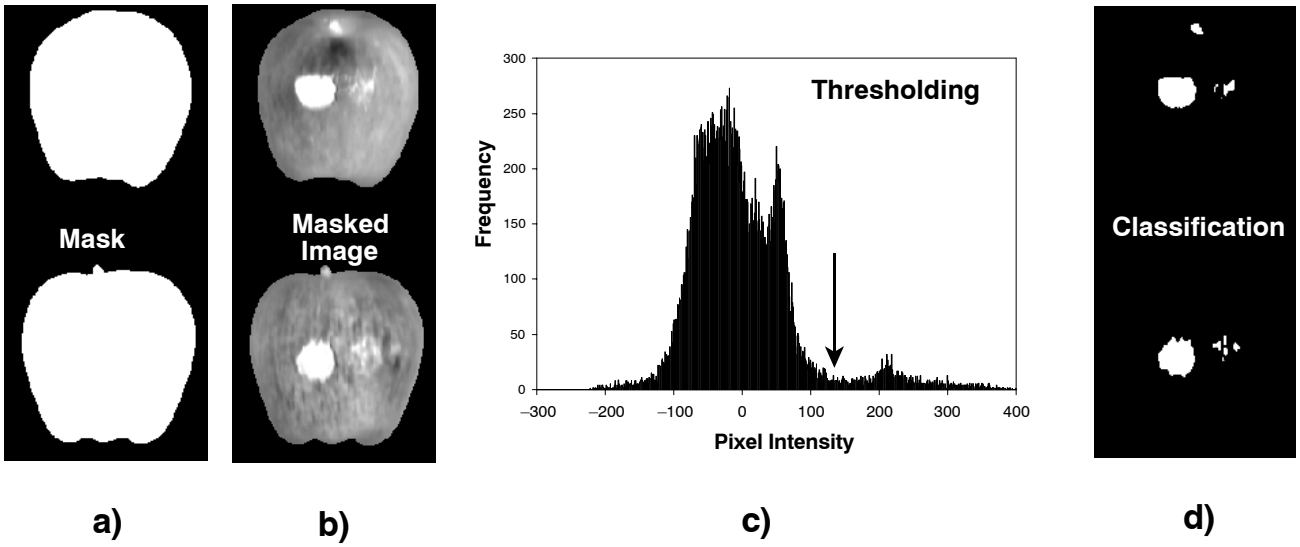

Figure 4. Key steps involved in classifying the principal component images of the feces–treated spots from the uncontaminated sample surfaces using a simple threshold method: (a) a mask for the sample surfaces determined by using a 851 nm image in conjunction with a simple threshold method, (b) masked PC–3 image of Red Delicious, (c) histogram of masked PC–3 image, and (d) classification results presented as a binary image.

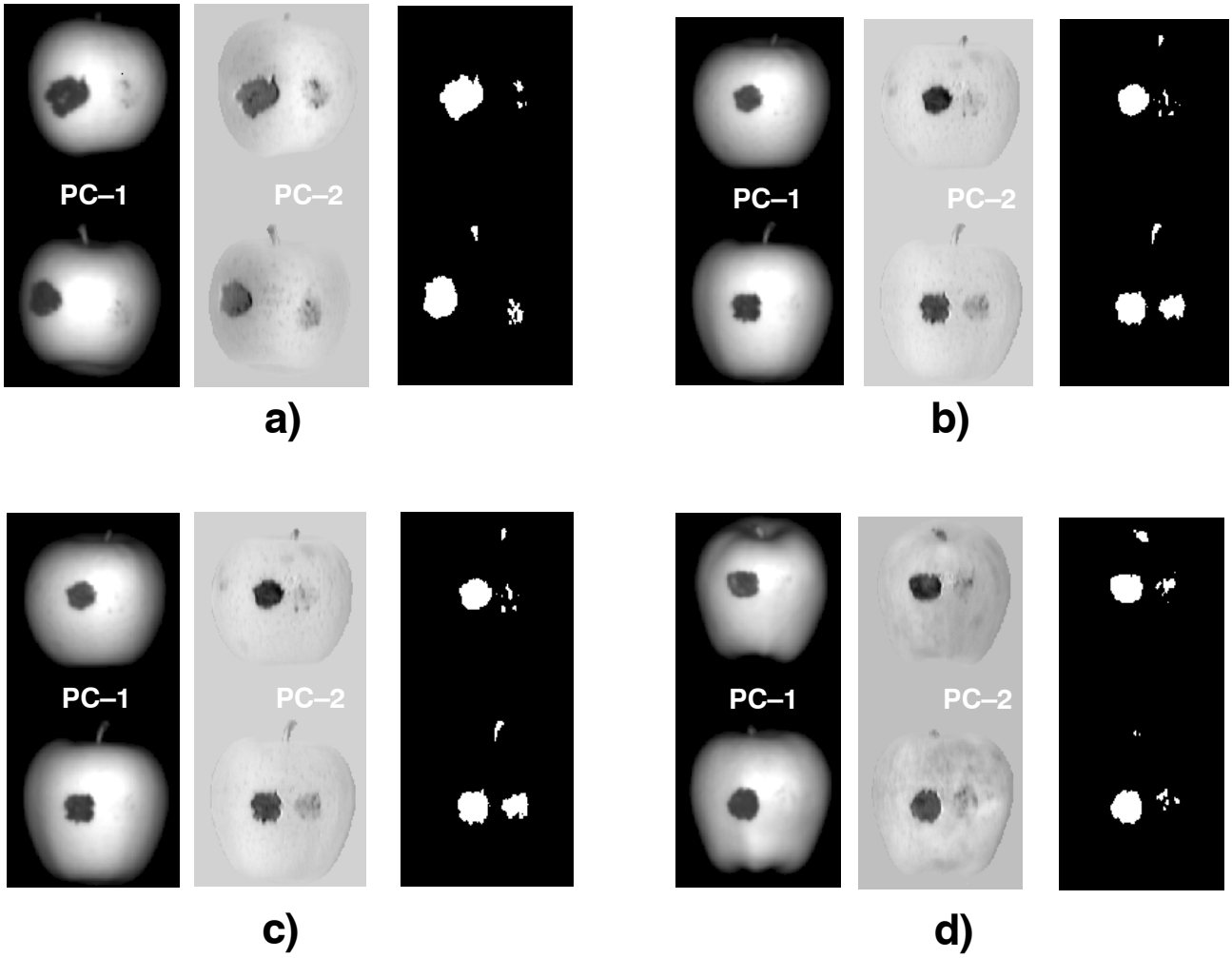

Figure 5. First and second principal component images obtained using 748 to 851 nm region (29 spectral channels) of the hyperspectral reflectance image data for (a) Fuji, b) Gala, (c) Golden Delicious, and (d) Red Delicious apples. Binary images shown in the third columns for each cultivar are the classification results using the simple threshold method on PC–2 images.

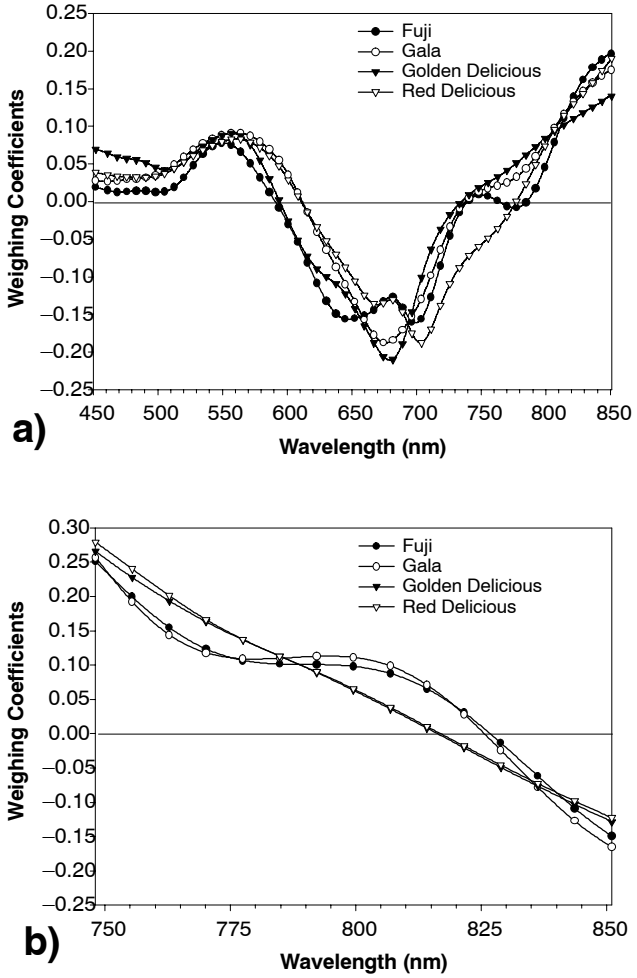

Figure 6. Weighing coefficients for: (a) the third PC images that resulted from using the entire spectrum (450 to 851 nm), and (b) the second PC images that resulted from using the NIR region of the spectrum (748 to 851 nm).

PCA of Optimal Spectral Band (Multispectral) Images

Based on the PCA of the hyperspectral images of fecal–contaminated apples, several spectral bands in the VIS–NIR regions were selected for further analyses. A number of (multispectral) transformations and algorithms (e.g., algebraic combinations, simple band ratios, second differences, normalized differences, and continuum removal) were examined in attempts to improve detection of fecal contamination spots (Kim et al., 2000). To evaluate the adequacy of the selected wavelengths under a consistent platform, the PCA was also performed with the use of only images at the previously identified wavelengths (table 1). Hence, the PCA using the three VIS–NIR bands and the two NIR bands was used to generate three and two (multispectral) PC images, respectively, for each cultivar.

The resultant multispectral PC images (i.e., PC–1 and PC–2 for the three bands, and PC–1 for the two bands; figures not shown) obtained from the multispectral PCA also showed characteristics similar in appearance to those of the corresponding PC images shown in figure 3 (PC–1 and PC–2) and figure 4 (PC–1), respectively, for all cultivars. With the use of the three multispectral bands, the PC–1 images mainly accounted for the decreases in intensity from the centers to the edges of apples, and the second PC images reflected the major color differences between the sun–exposed and shaded sides of apples. The first PC images from the two NIR bands also exhibited decreases in intensity from the centers to the edges of apples. These images appeared similar in form, if not actual brightness, to the corresponding PC images in figures 3 and 4, respectively. The resultant PC–3 and PC–2 images shown in figure 7 clearly demonstrate the effective delineation of the treated spots from the apple surfaces; however, the sensitivity for detecting thin smears was still much lower than for thick spots. This lack of sensitivity suggests that reflectance (imaging) techniques may be inadequate for reliable detection of thin contamination smears on apple surfaces. Note that the PC–2 images in this figure are inverted images of the actual PC–2 images, thus allowing for better comparisons between the PC–3 and PC–2 images.

For each cultivar, the results obtained by the use of the two selected NIR bands showed less spatial variation in intensities within and between apple surfaces compared to the results obtained by the three selected wavelengths in the VIS–NIR regions. This observation is more evident in image histograms for the PC–3 and PC–2 (fig. 8). For each cultivar, graphs on the left and right are for the PC–3 and PC–2 image histogram, respectively. For each plot, the larger pixel distribution observed on the left side is the pixel intensities of apple surfaces. Higher peak frequency and narrower width of the pixel distributions observed for the PC–2 as compared to the PC–3 plots are due to reduced spatial variations associated with apple surfaces. The smaller peaks on the right side of the individual histograms are due to fecal contamination. However, there exist overlapping pixel regions in the histograms between the treated spots and sample surfaces, especially for the thin fecal smears. With the use of the selected three bands, the PC–3 images resulted greater variations for normal apple surfaces compared to the PC–2 by the two NIR bands. However, a multispectral imaging system equipped with the three bands may provide both detection of fecal contamination and color sorting capability.

Table 1. Selected wavelengths (nm) based on the PCA of hyperspectral reflectance images in the entire spectrum region and in the NIR region under investigation. Spectral channel numbers are also provided in parentheses.

Apple Cultivar	VIS–NIR (450 to 851 nm)			NIR (748 to 851 nm)	
	Green	Red	NIR	NIR–1	NIR–2
Fuji	549.5 (37)	700.3 (79)	851.0 (119)	748.1 (91)	851.0 (119)
Gala	560.6 (40)	678.2 (72)	851.0 (119)	748.1 (91)	851.0 (119)
Golden Delicious	556.9 (39)	678.2 (72)	851.0 (119)	748.1 (91)	851.0 (119)
Red Delicious	560.6 (40)	703.9 (80)	851.0 (119)	748.1 (91)	851.0 (119)

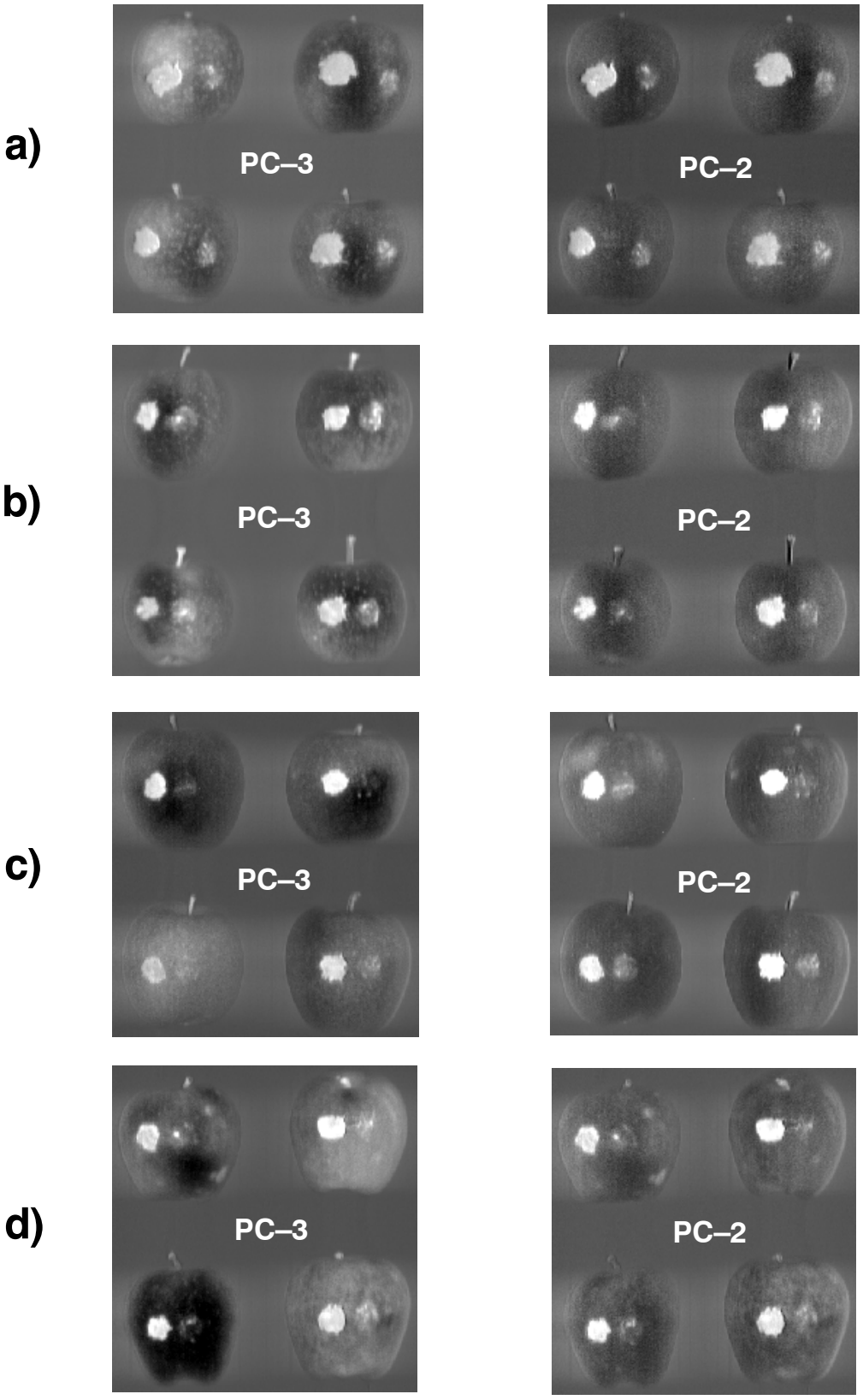

Figure 7. Principal component images for (a) Fuji, (b) Gala, (c) Golden Delicious, and (d) Red Delicious apples that show best delineation of the feces–treated spots from the uncontaminated apple surfaces. For each cultivar, images shown on the left are the PC–3 images obtained from PCA of the three selected VIS–NIR bands, and the images on the right are the PC–2 images yielded by the PCA of the two selected NIR bands. Note that results are shown with all four apples per cultivar.

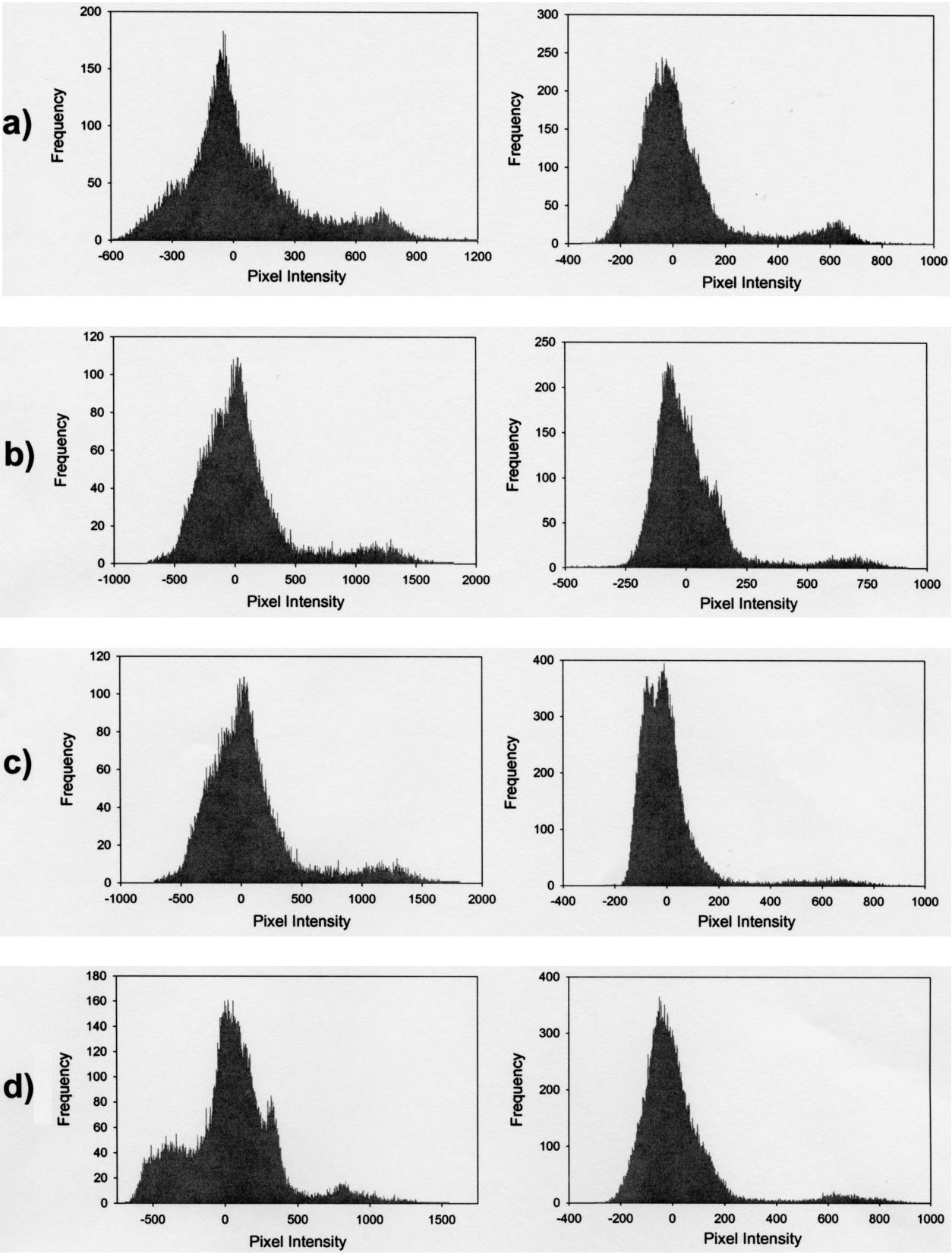

Figure 8. Image histograms showing pixel intensity vs. pixel frequency for the multispectral PC–3 and PC–2 images shown in figure 7.

It should be emphasized that the simple threshold method used earlier was not meant to be used as a classification method. A myriad of classification techniques are available. However, the number of apples examined in this study is inadequate for detailed evaluation of optimal classification schemes. The purpose of the study was to address the feasibility of using reflectance measurements for detection of fecal–contaminated apples. The results related to thin smears

suggests that reflectance measurements by themselves may not be adequate to detect low–level contamination. Furthermore, to rigorously test the use of multispectral bands, as defined in this investigation, would require quantitative application of feces to a large number of apples. It should also be remembered that stems often have reflectance characteristics similar to those of feces. Pattern recognition algorithms would allow stems to be ignored at the expense of some increase in computational complexity. One finding not currently addressed is that VIS–NIR and NIR PCA concomitantly selected the longest–available NIR band at 851 nm. This suggests that it might be worthwhile to examine wavelengths above 850 nm in a future study.

Conclusions

To detect fecal–contaminated apples, we presented a systematic approach using hyperspectral reflectance imaging technique in conjunction with the use of PCA to define several optimal wavelength bands. This was demonstrated in the presence of large variations (reflectance intensity) of normal apples due to the inherent surface morphology and skin colorations. This investigation illustrated that, with the use of the PCA, high spectral dimension reflectance images data were reduced to several optimal wavelengths (multispectral) images. We identified three VIS–NIR and, alternatively, two NIR wavelengths that could potentially be implemented in multispectral imaging systems for detection of fecal contamination on apples.

We can classify fecal contamination spots on apples for individual apple cultivars with the use of the single threshold method. However, the reflectance imaging method detected only a fraction of the thin feces spots, indicating a lack of sensitivity. Another optical sensing method available is fluorescence. A companion article describes the use of hyperspectral fluorescence imaging techniques, and the results suggest that the ability to detect fecal contamination on apples may be improved by using fluorescence instead of reflectance measurements. However, commercial apple imaging systems currently use reflectance measurements. Financial considerations, such as the cost of modifying existing systems as opposed to developing new systems for fluorescence measurements, militate for at least examining the potential for using reflectance measurements for detection. Even if results indicate lower sensitivity, the sensitivity may be adequate for implementation in a commercial system.

References

Burnett, S. L., J. Chen, and L. R. Beuchat. 2000. Attachment of *Escherichia coli* O157:H7 to the surfaces and internal structures of apples as detected by confocal scanning laser microscopy. *Applied Environ. Microbiology* 66: 4679–4687.

Chen, Y. R., K. Chao, and M. S. Kim. 2002. Future trends of machine vision technology for agricultural applications. *Comp. Elec. in Agric.* 36(2–3): 173–191.

Cody, S. H., M. K. Glynn, J. A. Farrar, K. L. Cairns, P. M. Griffin, J. Kobayashi, M. Fyfe, R. Hoffman, A. S. King, J. H. Lewis, B. Swaminathan, R. G. Bryant, and D. J. Vugia. 1999. An outbreak of *Escherichia coli* O157:H7 infection from unpasteurized commercial apple juice. *Annals of Internal Med.* 130: 202–209.

FDA. 2001. Hazard analysis and critical control point (HAACP): Procedures for the safe and sanitary processing and importing of juices. *Federal Registry* 66(13): 6137–6202.

Kim, M. S., K. Chao, Y. R. Chen, D. Chan, and P. M. Mehl. 2000. Hyperspectral imaging system for food safety: Detection of fecal contamination on apples. *Proc. SPIE* 4206: 174–184.

Kim, M. S., Y. R. Chen, and P. M. Mehl. 2001a. Hyperspectral reflectance and fluorescence imaging system for food quality and safety. *Trans. ASAE* 44(3): 721–729.

Kim, M. S., A. M. Lefcourt, and Y. R. Chen. 2001b. Determination of optimal fluorescence bands for detection of fecal contamination on agricultural commodities. *J. Food Prot.* (in submission).

Lu, R., and Y. R. Chen. 1998. Hyperspectral imaging for safety inspection of foods and agricultural products. *Proc. SPIE* 3544: 121–133.

Mehl, P. M., K. Chao, M. S. Kim, and Y. R. Chen. 2002. Detection of contamination on selected apple cultivars using hyperspectral and multispectral image analysis. *Applied Eng. in Agric*. 18(2): 219–226.

Mercier, J., and C. L. Wilson. 1994. Colonization of apple wounds by naturally occurring microflora and introduced *Candida olephila* and their effect on infection by *Botrytis cinerea* during storage. *Biol. Control*. 4: 138–144.

Miller, W. M., J. A. Throop, and B. L. Upchurch. 1998. Pattern recognition models for spectral evaluation of apple blemishes. *Postharvest Biology and Technology* 14: 11–20.

Tao, Y. 1997. Closed–loop search method for on–line automatic calibrations of multi–camera inspection systems. *Trans. ASAE* 41(5): 1549–1555.

Throop, J. A., D. J. Aneshansley, and B. L. Upchurch. 1995. An image processing algorithm to find new and old bruises. *Applied Eng. in Agric.* 11(5): 751–757.

Upchurch, B. L., H. A. Affeldt, W. R. Hruschka, K. H. Norris, and J. A. Throop. 1990. Spectrophotometric study of bruises on whole Red Delicious apples. *Trans. ASAE* 33(2): 585–589.

Upchurch, B. L., J. A. Throop, and D. J. Aneshansley. 1994. Influence of time, bruise type, and severity on near–infrared reflectance from apple surfaces for automatic bruise detection. *Trans. ASAE* 37(5): 1571–1575.